Green Chemistry

Accepted Manuscript

This article can be cited before page numbers have been issued, to do this please use: C. Han, X. Yang, G. Gao, J. Wang, H. Lu, J. Liu, M. Tong and X. Liang, *Green Chem.*, 2014, DOI: 10.1039/C4GC00367E.

ROYAL SOCIETY OF CHEMISTRY

www.rsc.org/greenchem

View Article Online
DOI: 10.1039/C4GC00367E

Graphical abstract

Selective oxidation of methanol to methyl formate on catalysts of Au-Ag alloy nanoparticles supported on titania under UV irradiation †

Chenhui Han, Xuzhuang Yang*, Guanjun Gao, Jie Wang, Huailiang Lu, Jie Liu, Min Tong and Xiaoyuan Liang

Au-Ag alloy nanoparticles on titania exhibit superior photocatalytic performance in selective oxidation of methanol to methyl formate.

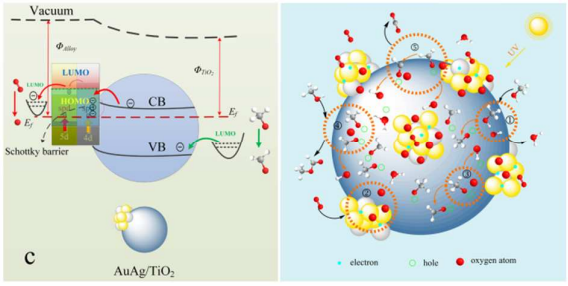

View Article Online
DOI: 10.1039/C4GC00387E

Journal Name

RSCPublishing

ARTICLE

Selective oxidation of methanol to methyl formate on catalysts of Au-Ag alloy nanoparticles supported on titania under UV irradiation †

Chenhui Han, Xuzhuang Yang*, Guanjun Gao, Jie Wang, Huailiang Lu, Jie Liu, Min Tong and Xiaoyuan Liang

Cite this: DOI: 10.1039/x0xx00000x

Received 00th January 2012,
Accepted 00th January 2012

DOI: 10.1039/x0xx00000x

www.rsc.org/

We find that the Au-Ag alloy nanoparticles supported on titania exhibit superior methanol conversion and methyl formate selectivity for selective oxidation of methanol by low partial pressure oxygen in air under UV irradiation in the 15°C - 45°C temperature range, with the highest methanol conversion above 90% and the highest selectivity to methyl formate above 85%. The only by-product definitely detected is CO_2. The superior photocatalytic performance of the catalyst is closely related to the special structure of the catalyst and the electronic property of the alloy, which reduce the recombination of the photo-excited electron-hole pairs by transferring the photo-exited electrons in time from the conduction band of titania to the alloy on the one hand, and elevate the negative charge level of the alloy surface by the *spd* hybridization, the formation of Schottky barriers, the electron transfer from the conduction band of titania to the metal as well as the interband and intraband electron transitions under UV irradiation on the other hand. The photo-generated holes are responsible for the oxidation from methanol to coordinated methoxy, from coordinated methoxy to coordinated formaldehyde and finally to carbon dioxide. The methyl formate selectivity is relevant to the density of the surface methoxy. To enhance the electron-hole separation efficiency is beneficial to the formation of the coordinated methoxy and coordinated formaldehyde and thus the selectivity to methyl formate. The negative charges on the surface of the metal are responsible for the dissociation of oxygen, which is the rate-determining step during the reaction. The dissociative oxygen repels the water molecules formed from the surface hydroxyls and refills the oxygen vacancies on the surface of titania. The surface oxygen is the acceptor of the hydrogen dissociated from methanol and/or methoxy and thus beneficial to the formation of the coordinated methoxy and coordinated formaldehyde. The oxygen partial pressure remarkably influences the methanol conversion and the methyl formate selectivity. The light intensity has only remarkable impact on the methanol conversion but not on the methyl formate selectivity. These findings provide useful insight into the design of catalysts for selective oxidation of methanol to methyl formate in a more green way.

Introduction

Methyl formate is an important intermediate in the chemical industry, which can be used to produce formic acid, formamides, acetic acid and ethylene glycol etc.[1-4]. The selective oxidation of methanol is one of the main routes for the synthesis of methyl formate[2-6]. Ai M.[4] reported this reaction on SnO_2-MoO_3 in 1982. Tronconi E. et al [2] and Ahmed S. E. et al[3] extensively studied vanadium-titanium oxides for the selective oxidation of methanol to methyl formate in 1987 and 1989, respectively. Liu H. et al[5] reported in 2005 that RuO_2 domains supported on SnO_2, ZrO_2, TiO_2, Al_2O_3, and SiO_2 were active to the selective oxidation of methanol and the catalysts supported on SnO_2, ZrO_2 and TiO_2 had better selectivity to methyl formate. Liu J. et al[7] reported that the selective oxidation of methanol to methyl formate occurred on ReO_x/CeO_2 at 500 K in 2008. Zhao Y. et al[8] observed five products including methyl formate on V_2O_5/ZrO_2-Al_2O_3 in 2013. It is the common feature for catalysts of metal oxides to have multi-by-products under the thermal condition, which, apparently, will increase the cost for the subsequent separation. It is noteworthy that Wittstock A. et al[6] prepared the nanoporous gold catalyst by dealloying Ag from an Au-Ag alloy to investigate the selective oxidation of methanol in 2010, and found that the selectivity toward methyl formate was close to 100% with 10% conversion of methanol at 20 °C. The conversion of methanol to methyl formate increased to about 45% at 65 °C but the selectivity to methyl formate decreased to about 80%. The locally "less noble" Au resulted

View Article Online
DOI: 10.1039/C4GC00367E
Journal Name

from the local change of the d-band structure in the dilute Au-Ag alloy and/or the residual Ag in the alloy were supposed to be the active sites on which oxygen was dissociated.

In recent years, the selective oxidation of methanol to methyl formate on photocatalysts has attracted great attention of researchers due to its ambient reaction condition and high yield of methyl formate[9, 10]. Kominami H.[9] reported that methanol could be selectively oxidized to methyl formate with the selectivity up to 90% from 298 K to 523 K on an anatase titania (ST-01) under UV irradiation, and the conversion of methanol to methyl formate was 8% to 28%. In our previous work[10], silver catalysts supported on commercial P25 and silica were found to be active to the selective oxidation of methanol to methyl formate in liquid phase, but the roles of silver nanoparticles on different supports were different. Those on P25 promoted the reaction through removing the photo-excited electrons from the surface of titania to extend the hole-electron lifetime, and the localized surface plasma resonance (LSPR) of the silver nanoparticles on silica was supposed to be responsible for the formation of methyl formate.

Titanium dioxide is the most popular and well-studied photocatalyst due to its high oxidizing capability, good stability, low cost, and non-toxic properties[11]. However, its photocatalytic efficiency which depends on the recombination rate of photo-excited holes and electrons is limited due to the lifetimes of them are very short, only a few nanoseconds in the absence of corresponding scavengers[11, 12]. Numerous studies have been carried out to improve the photocatalytic efficiency including the noble metal modification[12-21]. Silver and gold are the most commonly used noble metal modifiers due to their stable chemistry and good performance of electron traps[14, 20, 21]. It has been reported that Schottky barrier exists at the interface between metal and semiconductor, and the metals such as silver or gold nanoparticles can scavenge the photo-excited electrons from the surface of semiconductor, reducing the electron-hole recombination[13-15, 18, 19, 21]. In addition, silver and gold nanoparticles exhibit extraordinary electronic property under irradiation. They can introduce a strong local electronic field in the vicinity of the nanoparticles due to the LSPR under visible light irradiation[10, 21-25], which is believed being capable of inducing or promoting some reactions[10, 26-29]. On the other hand, the interband and intraband electron transition can be induced under UV irradiation[27, 28], which can enhance the electronegativity on the surface of metal and thus favorable to the electrophilic reactions.

Table 1 Nominal and actual metal contents and Au/Ag ratios in the catalysts

catalysts	M_t/Ti [at.%][a]	M_t/Ti [at.%][b]	Au/Ag R_{at}[a]	Au/Ag R_{at}[b]	error [%][c]
Au/TiO_2	2.30	2.56	1/0	1/0	10.16
Ag/TiO_2	2.43	2.56	0/1	0/1	5.08
$AuAg(1:3)/TiO_2$	2.25	2.56	1/2.5	1/3	12.11
$AuAg(1:1)/TiO_2$	2.18	2.56	1/0.8	1/1	14.84
$AuAg(3:1)/TiO_2$	2.09	2.56	3.4/1	3/1	18.36

M_t, total moles of gold and silver; R_{at}, atom ratio; [a] Actual value ; [b] Nominal value ; [c] Percentage of the difference between the actual value and the nominal value accounting for the nominal value (Au+Ag)/Ti.

The band structure and electronic property of the Au-Ag alloy nanoparticles are different from the pure metals[30-32]. The supported alloy nanoparticles often exhibit outstanding catalytic performance in a lot of thermal catalytic and photocatalytic reactions[33-37]. However, supported Au-Ag alloy nanoparticles have not ever been used in photocatalytic selective oxidation of methanol to methyl formate.

In this study, the catalysts of Au, Ag, Au-Ag alloy and dealloyed Au nanoparticles supported on titania were prepared, and the photocatalytic performance for the selective oxidation of methanol to methyl formate in gaseous phase was investigated under the irradiation of UV-light. The objectives of this study are to investigate the selective oxidation performances from methanol to methyl formate of the nanoparticles of Au, Ag and Au-Ag alloys at different ratios supported on titania, as well as the reaction mechanisms of the catalysts.

Results and discussion

The nominal molar content of the noble metals in the catalyst was designed as 2.5%. For the catalyst of Au-Ag alloy, the nominal content of metals was calculated by the total moles of gold and silver in the catalyst divided by the total moles of gold, silver and titania in the catalyst. The actual noble metal content in the catalyst was determined by the energy dispersive spectroscopy (EDS) obtained from the microanalysis system equipped on the scanning electron microscopy (SEM). Table 1 lists the nominal and actual total noble metal contents as well as the Au/Ag ratios in the catalysts. The actual metal loading was slightly less than the nominal loading in each catalyst because of the metal loss during washing. The actual Au/Ag ratio in each catalyst was slightly different from the nominal one as well. The recipe of each catalyst is listed in Table 1s.

Gold and silver are very easy to form a solid solution alloy because they are of the like valence and have essentially identical lattice constants, thus neither the volume nor the valence effects contributes significantly to the alloy behavior[30]. Gold, silver and their alloy are attributed to the cubic crystal system and the Fm-3m space group. The diffraction peaks of the same lattice plane for Au, Ag and Au-Ag alloy at different Au/Ag ratios are almost at the same position of the 2 theta (diffraction angle), such as (200) at about 44.6°, (220) at about 64.6° and (311) at about 77.5° (See Fig. 1a). The diffractions of the alloy in the uncalcined catalyst of $AuAg(1:1)/TiO_2$-UC could not be identified in the pattern because of the poor crystallinity of the noble metals on titania before calcination (Fig. 1b), although gold and silver existed in metallic state in this condition. The temperature and the duration of calcination had little influence on the phase of the noble metals in the catalyst, not even the dealloying process to remove most of silver by the acid leaching method.

However, the temperature and the duration of calcination as well as the dealloying process remarkably influence the morphology, the particle size distribution and even the electron configuration of the noble metals on titania. During the preparation, the protecting agent such as PVA was not used because the molecules of the protecting agent coating the surfaces of silver nanoparticles are difficult to be removed and unfavorable to the subsequent substitution reaction between gold and silver. As a result, the sizes of the noble metal nanoparticles on titania were larger and the size distributions were broader (Fig. 2), compared to those using a protecting agent. The inset in the lower right corner of each image in Fig.2 is the size distribution of the noble metal nanoparticles on

View Article Online
DOI: 10.1039/C4GC00387E

Journal Name

RSCPublishing

ARTICLE

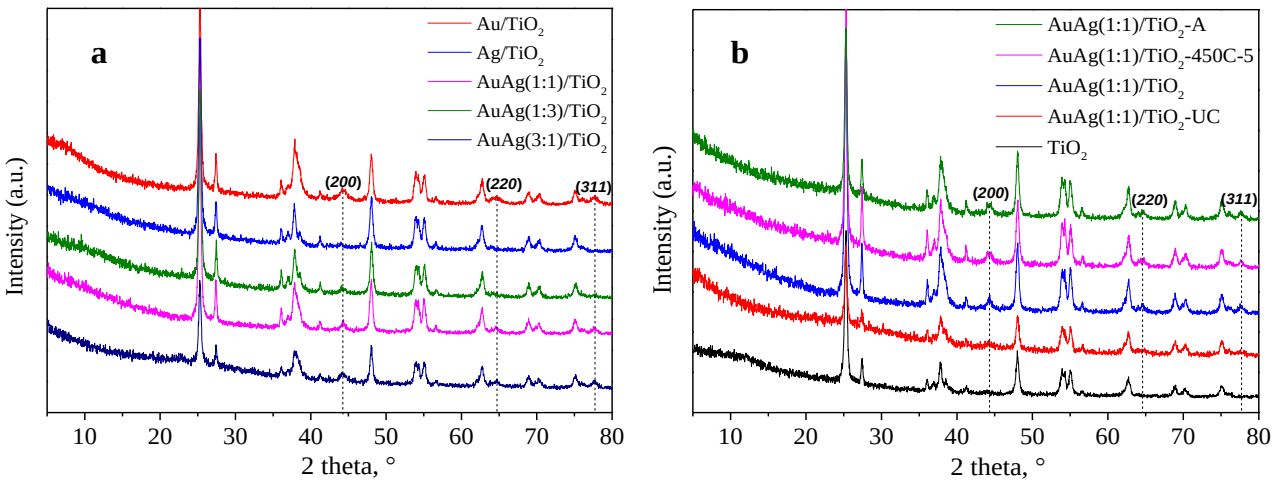

Fig. 1 XRD patterns of P25 and catalysts of Au, Ag and Au-Ag alloy nanoparticles supported on P25. TiO_2 was the pure P25. Au/TiO_2 and Ag/TiO_2 were pure Au and Ag supported on P25, respectively. $AuAg(1:1)/TiO_2$, $AuAg(3:1)/TiO_2$ and $AuAg(1:3)/TiO_2$ were the catalysts with different Au/Ag ratios calcined at 400 °C. $AuAg(1:1)/TiO_2$-450C-5 was the catalyst with the Au/Ag ratio 1:1 and calcined at 450 °C for 5 h. $AuAg(1:1)/TiO_2$-UC was the uncalcined catalyst with the Au/Ag ratio 1:1. $AuAg(1:1)/TiO_2$-A was the dealloyed $AuAg(1:1)/TiO_2$ catalyst.

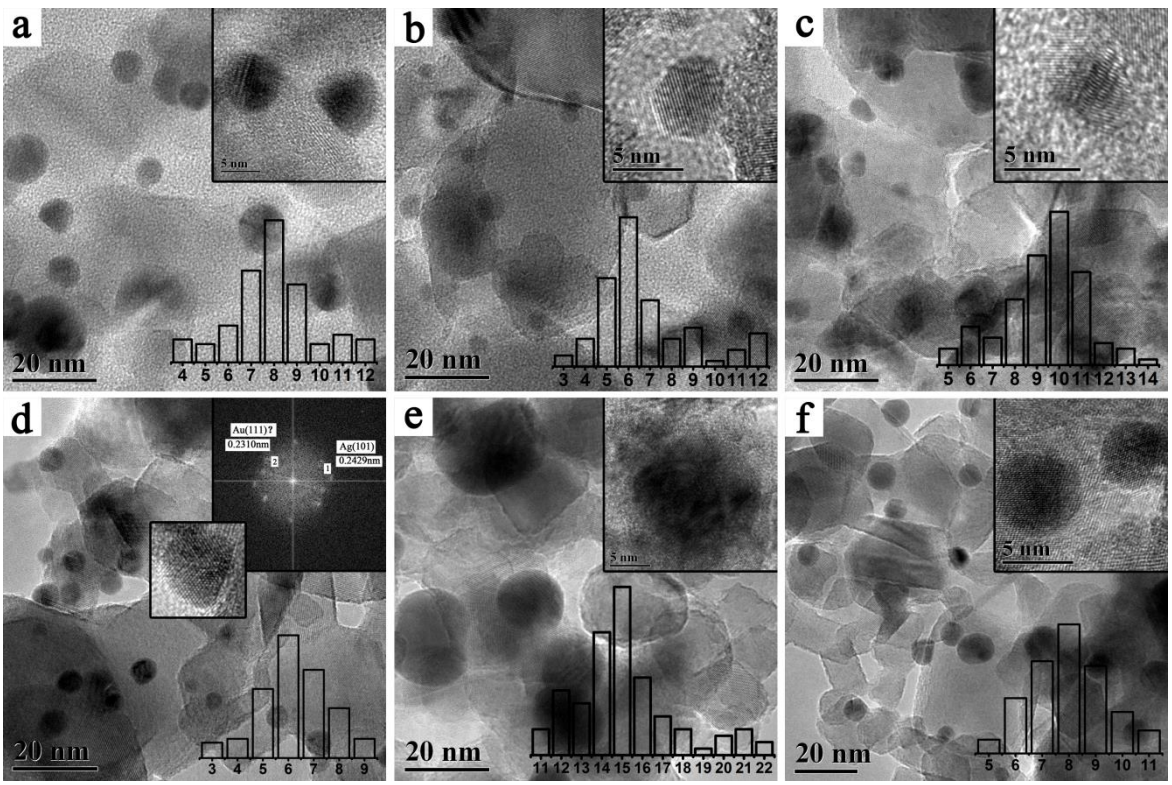

Fig. 2 TEM images of catalysts and size distributions of noble metal nanoparticles on support. (a) Au/TiO_2 and (b) Ag/TiO_2 were pure Au and Ag supported on P25, respectively. (c) $AuAg(1:1)/TiO_2$ was the catalysts calcined at 400 °C with the Au/Ag ratio 1:1. (d) $AuAg(1:1)/TiO_2$-UC was the uncalcined catalyst with the Au/Ag ratio 1:1. (e) $AuAg(1:1)/TiO_2$-450C-5 was the catalyst with the Au/Ag ratio 1:1 and calcined at 450 °C for 5 h. (f) $AuAg(1:1)/TiO_2$-A was the dealloyed $AuAg(1:1)/TiO_2$ catalyst.

View Article Online
DOI: 10.1039/C4GC00367E

Journal Name

RSCPublishing

ARTICLE

titania, and that in the upper right corner is the HRTEM image or the electron diffraction pattern of the selected area in the HRTEM image of the noble metal nanoparticles on the sample. The size of gold nanoparticles on Au/TiO_2 was slightly larger than that of silver nanoparticles on Ag/TiO_2, and smaller than that of the Au-Ag alloy nanoparticles on $AuAg(1:1)/TiO_2$. Before calcination, the gold and silver on titania existed in a close contact core/shell structure (See the inset HRTEM image in Fig. 2d), and the low crystallinity of gold and silver at this stage made them unable to be detected by XRD as well (See Fig. 1b). The alloy nanoparticles on titania grew larger and the sizes of them distributed in a broader range when elevating the calcination temperature (See Fig. 2e). After free corrosion in a diluted nitrate acid solution, most of the silver species were leached out and the remaining gold nanoparticles shrank to smaller ones (See Fig. 2f).

The electronic property of gold or silver nanoparticles is quite different from that of other metal nanoparticles. The LSPR of the electrons in the conduction band of them can be induced by the interaction with an electromagnetic field[21, 24, 25], which can be detected by observing the strong absorption band in the visible region. The resonance frequencies as well as the width of the plasmon absorption bands depend on the size, the shape and the electron density in conduction band of the nanoparticles[24, 25, 38]. Fig. 3a shows the LSPR absorptions of the colloid nanoparticles of Au, Ag and Au-Ag alloy with different Au/Ag ratios. The absorption band of silver nanoparticles peaks at 400 nm of the wavelength and that of gold nanoparticles peaks at 530 nm[17, 19, 21, 39]. The peaks in the absorption bands attributed to Au-Ag alloy nanoparticles are between 400 nm and 530 nm, which shift to the longer wavelength direction with increasing the Au content in the alloy. The absorption band width of the alloy nanoparticles is broader than that of the pure Au or Ag nanoparticles, and the intensity of the absorption bands increases with elevating the Ag content in the alloy. The absorption differences are more possibly resulted from the variations of the electronic configurations in the conduction bands of the alloy nanoparticles, in addition to the size and shape effects. When Au is alloyed with Ag the flow of *s* charge onto Au sites is accompanied by a compensating depletion of d charge[30]. The DFT (density function theory) calculation also indicates that the electron transfer from 5d and 6s to 6p for Au and 4d and 5s to 5p for Ag occurs on Au-Ag alloy[32]. The details are discussed in the following sections. The absorption bands, however, change greatly for the titania supported noble metal nanoparticles (Fig. 3b, c). The peaks of the absorption bands shift to the longer wavelength direction for all samples. Especially, all absorption peaks of the three titania supported alloy samples shift to 550 nm, meanwhile the absorption bands of them are broadened as well (Fig. 3b). The changes of the absorption bands for the titania supported noble metal nanoparticles indicate the changes of the electronic configurations in the conduction bands of these noble metal nanoparticles. The formation of Schottky barriers between the noble metal nanoparticles and titania is probably responsible for these variations, which results in the electron flow from titania to noble metal nanoparticles[13, 14, 18, 21]. Detailed discussions can

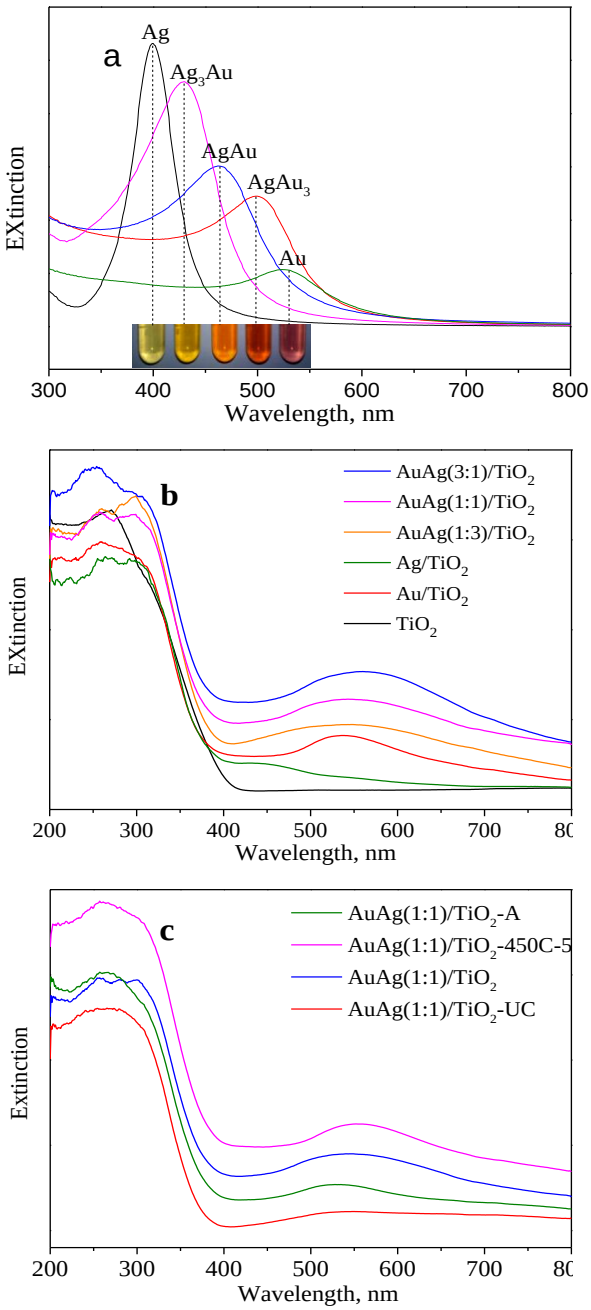

Fig. 3 UV-visible spectra of noble metal colloid nanoparticles and catalysts. (a) Spectra of Au, Ag and Au-Ag alloy nanoparticles in liquid, the alloy nanoparticles with Au/Ag ratios of 1:1 (AgAu), 1:3 (Ag_3Au) and 3:1 ($AgAu_3$); (b) Spectra of titania (TiO_2), pure Au (Au/TiO_2) and Ag (Au/TiO_2) nanoparticles on titania, alloy nanoparticles with Au/Ag ratios of 1:1 ($AuAg(1:1)/TiO_2$), 1:3 ($AuAg(1:3)/TiO_2$) and 3:1 ($AuAg(3:1)/TiO_2$) on titania; (c) Spectra of the alloy nanoparticles with the Au/Ag ratio of 1:1 on titania, calcined at different tempratures. $AuAg(1:1)/TiO_2$-450C-5 was the catalyst calcined at 450 °C for 5 h. $AuAg(1:1)/TiO_2$-UC was the uncalcined catalyst. $AuAg(1:1)/TiO_2$-A was the dealloyed $AuAg(1:1)/TiO_2$ catalyst.

View Article Online
DOI: 10.1039/C4GC00387E

be found in the following sections. The calcination temperature remarkably influences the visible light absorption by the alloy nanoparticles on titania (Figure 3c). The uncalcined catalyst of AuAg(1:1)/TiO_2 -UC exhibits a weak visible light absorption band. With elevating the calcination temperature, the intensity of the absorption bands is strengthened. Apparently, calcination is beneficial to the formation of Au-Ag alloy or the new energy band structure of the Au-Ag alloy. After removing most of the silver by dealloying, the absorption band of AuAg(1:1)/TiO_2-A blue shifts, close to the band of gold nanoparticles on titania.

The differences of the electronic configurations of the noble metal nanoparticles supported on titania remarkably influence photocatalytic performances of these catalysts. Titania itself was active to selective oxidation of methanol to methyl formate under UV irradiation. The total conversion of methanol on titania was about 10% - 27% and the selectivity to methyl formate was about 50% - 56% in the 15 °C - 45 °C temperature range. However, the total conversion and the methyl formate selectivity increased sharply after loading the nanoparticles of silver, gold or the alloy of them on titania (Fig. 4a-d). The total conversion of methanol on Au/TiO_2 was about 50% - 65% and that on Ag/TiO_2 was about 35% - 75%, but the selectivity to methyl formate on Ag /TiO_2 was 75% - 80%, higher than that on Au/TiO_2, which was about 65% - 75%. The total conversions of methanol on the Au-Ag alloy catalysts were far higher than that on the pure gold or silver catalyst. The catalyst of AuAg/(1:1)/TiO_2 had the best methanol conversion from 75% to 90% and the best methyl formate selectivity from 80% to 85% in the 15 °C – 45 °C temperature range. The calcination temperature remarkably influenced the methanol conversion and the methyl formate selectivity of the Au-Ag alloy catalyst. The catalyst calcined at 400°C for 1 h had the best methanol conversion and methyl formate selectivity. The uncalcined catalyst had a moderate methanol conversion and it became worse when the catalyst was calcined at 450°C for 5h. The methyl formate selectivity of the uncalcined catalyst was slightly higher than that of the catalyst calcined at 450°C for 5 h in the 15 °C - 40 °C temperature range, but it was contrary at 45 °C. The remove of silver from the AuAg/(1:1)/TiO_2 catalyst by dealloying led to a sharp decrease of the methanol conversion and a slightly decrease of the methyl formate selectivity.

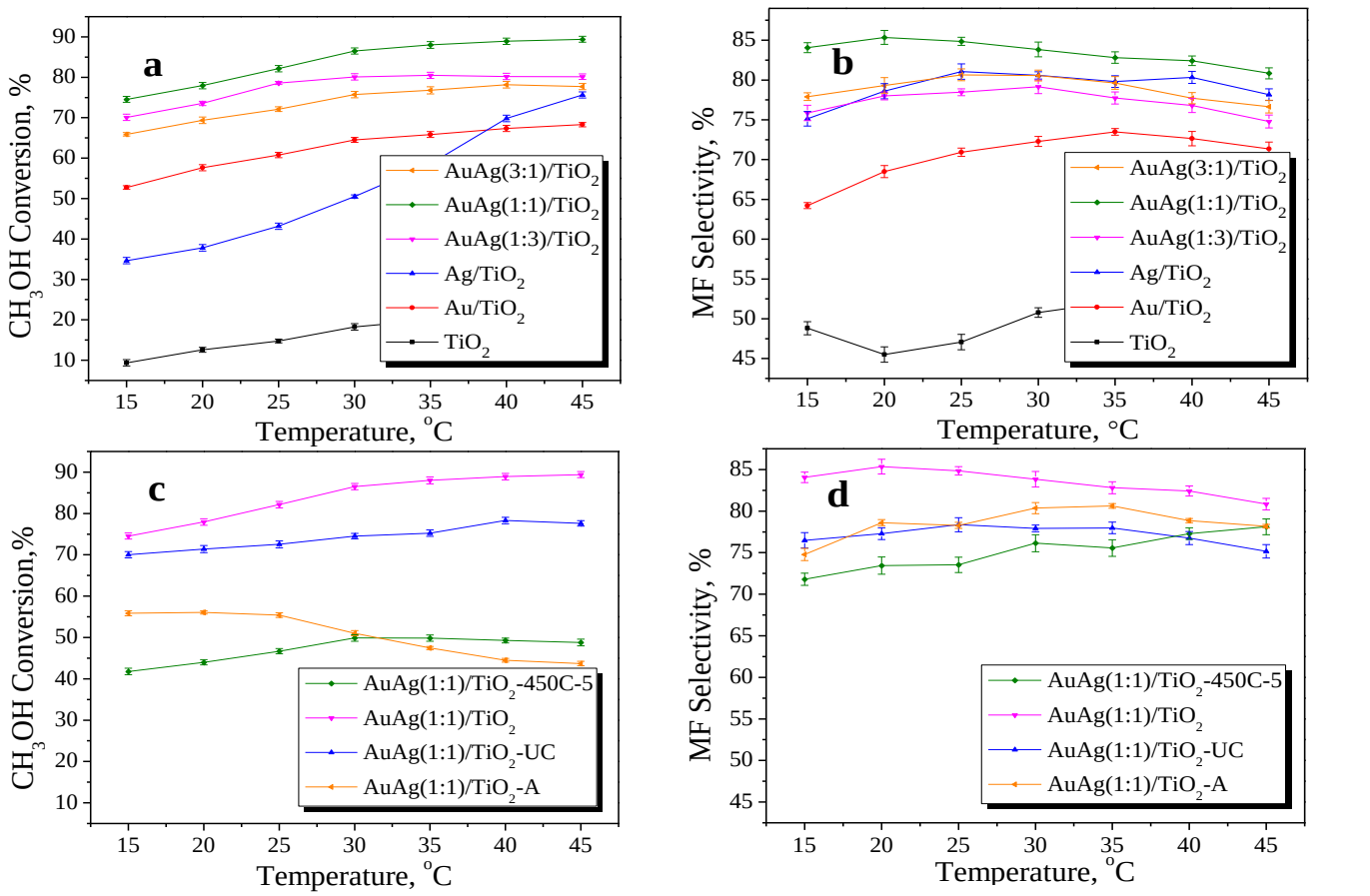

Fig. 4 Conversion of methanol (a, c) and selectivity to methyl formate (b, d) on catalysts. (a, b) titania (TiO_2), pure Au (Au/TiO_2) and Ag (Au/TiO_2) nanoparticles on titania, alloy nanoparticles with Au/Ag ratios of 1:1 (AuAg(1:1)/TiO_2), 1:3 (AuAg(1:3)/TiO_2) and 3:1 (AuAg(3:1)/TiO_2) on titania; (c, d) AuAg(1:1)/TiO_2-450C-5, calcined at 450 °C for 5 h, AuAg(1:1)/TiO_2-UC, uncalcined catalyst, AuAg(1:1)/TiO_2-A, dealloyed AuAg(1:1)/TiO_2.

The methyl formate formation rate is an overall indicator for evaluating the catalytic performance of the catalyst. The maximum methyl formate formation rate on ST-01 in a continuous flow reactor under UV irradiation was less than 1.5 mmol.g^{-1}.h^{-1} [9], and that on CuO-TiO_2 for the reduction of CO_2 in liquid methanol under UV irradiation in a batch reactor was less than 1.6 mmol.g^{-1}.h^{-1} [40]. In our previous work on Ag/TiO_2 and Ag/SiO_2 in a batch reactor in liquid phase, the maximum

View Article Online
DOI: 10.1039/C4GC00367E
ARTICLE Journal Name

methyl formate formation rate attained to 23 mmol.g^{-1}.h^{-1} [10]. The methyl formate formation rate on a nanoporous gold catalyst in a continuous flow reactor was about 40.0 mmol.g^{-1}.h^{-1}, which was the highest value so far for the selective oxidation of methanol to methyl formate in literature[6]. The methyl formate formation rates of the catalysts in this work are shown in Fig. 5. The maximum methyl formate formation rate on P25 was 4.6 mmol.g^{-1}.h^{-1}, and that on Au/TiO_2 was 15 mmol.g^{-1}.h^{-1} and on Ag/TiO_2 was 18 mmol.g^{-1}.h^{-1}. The methyl formate formation rates on the alloy catalysts were higher than those on the pure noble metal catalysts. The AuAg/(1:1)/TiO_2 had the highest methyl formate formation rate in the temperature range from 15 °C to 45 °C, with the maximum of 23 mmol.g^{-1}.h^{-1} at 30 °C. The uncalcined catalyst AuAg/(1:1)/TiO_2-UC had a moderate methyl formate formation rate, with the maximum of 18 mmol.g^{-1}.h^{-1} at 40 °C; however, the methyl formate formation rate decreased sharply to 11 mmol.g^{-1}.h^{-1} on AuAg/(1:1)/TiO_2-450C-5 that was calcined at 450 °C for 5 h and to 13 mmol.g^{-1}.h^{-1} on the dealloyed catalyst AuAg/(1:1)/TiO_2-A. However, if the methyl formate formation rate was calculated by per unit noble metal, the highest value in this study was 10 times more than that in literature[6]. (See Fig. s3)

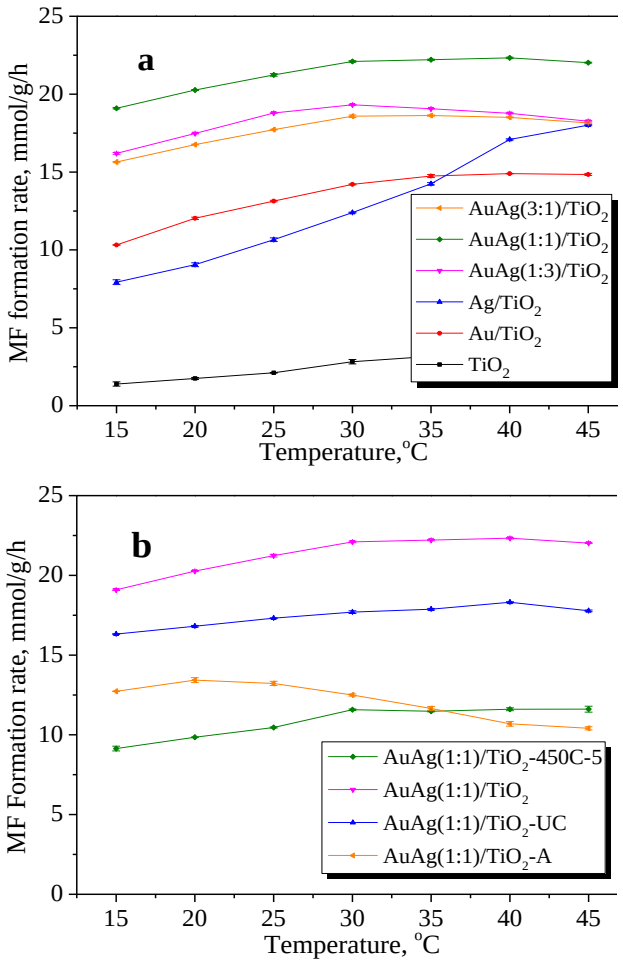

Fig. 5 Formation rate of methyl formate on catalysts. (a,) titania (TiO_2), pure Au (Au/TiO_2) and Ag (Au/TiO_2) nanoparticles on titania, alloy nanoparticles with Au/Ag ratios of 1:1 (AuAg(1:1)/TiO_2), 1:3 (AuAg(1:3)/TiO_2) and 3:1 (AuAg(3:1)/TiO_2) on titania; (b) AuAg(1:1)/TiO_2-450C-5, calcined at 450 °C for 5 h, AuAg(1:1)/TiO_2-UC, uncalcined catalyst, AuAg(1:1)/TiO_2-A, dealloyed AuAg(1:1)/TiO_2.

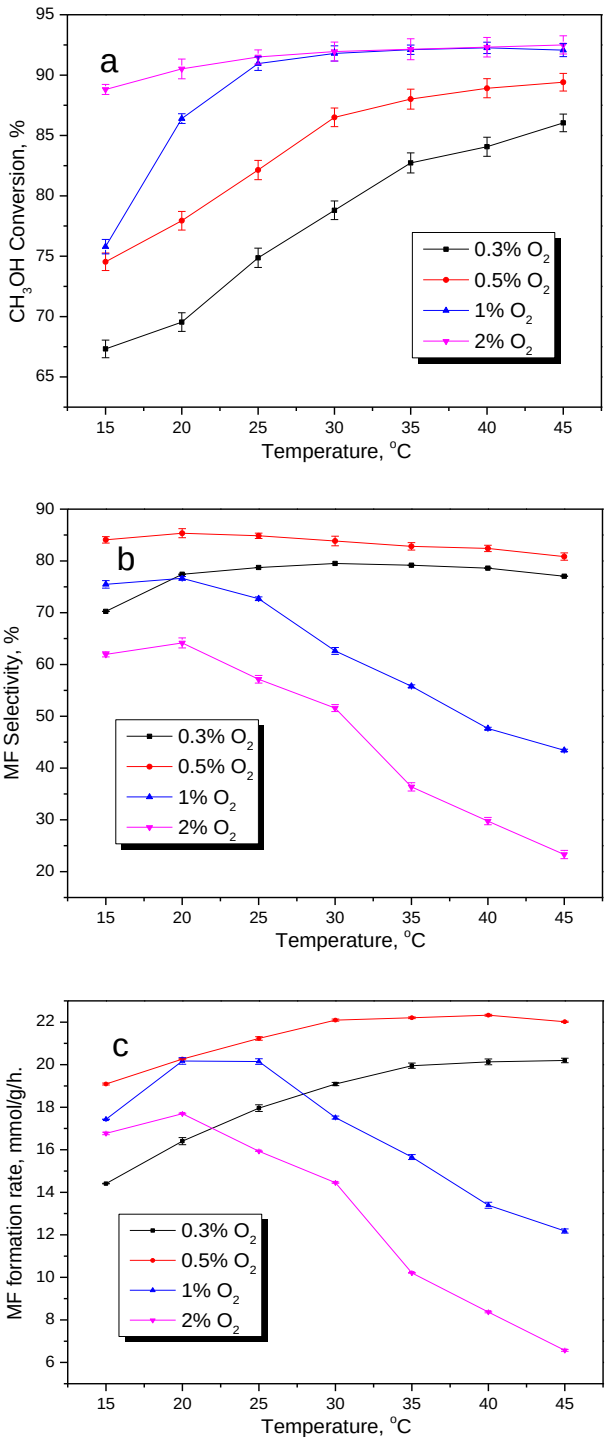

Fig. 6 Conversion of methanol (a), selectivity of methyl formate (b) and formation rate of methyl formate (c) on the catalyst of AuAg(1:1)/TiO_2. The volume content of methanol in the feed gas was 1 vol.%.

The operation conditions influence the photocatalytic performance as well in addition to the physicochemical properties of catalysts, especially for the oxygen partial pressure and the light intensity. Fig. 6 shows the impact of oxygen partial pressure on the conversion of methanol, the selectivity of methyl formate and the formation rate of methyl

formate. The stoichiometric ratio of methanol to oxygen for partial oxidation of methanol to methyl formate is 2. The stoichiometric volume content of oxygen in the feed gas is 0.5 vol.% when the methanol volume content is 1 vol.%. The conversion of methanol increased with increasing the oxygen content from 0.3 vol.% to 2 vol.% in the temperature range from 15 °C to 30 °C. In the case that oxygen in the feed gas exceeded the stoichiometric ratio, the conversion of methanol attained to a constant comparable level in the temperature range from 30 °C to 45 °C.

However, the selectivity of methyl formate reached the maximum in the whole temperature range when oxygen was at the stoichiometric ratio, and it decreased with increasing the oxygen content when oxygen was over the stoichiometric ratio. When the reaction was performed with oxygen below the stoichiometric ratio, the selectivity of methyl formate was higher than that performed with oxygen-rich feed gas but lower than that performed with oxygen at the stoichiometric ratio. When oxygen in the feed gas was below or at the stoichiometric ratio, the methyl formate formation rate increased with elevating the reaction temperature from 15 °C to 45 °C, but it rose first from 15 °C to 20 °C then declined sharply from 20 °C to 45 °C, and decreased with increasing the oxygen stoichiometric ratio, in the condition that the oxygen content was over the stoichiometric ratio.

Apparently, the oxygen partial pressure is a sensitive factor for the reaction, which determines not only the reaction rate but also the product distribution and will be discussed in detail in the following section.

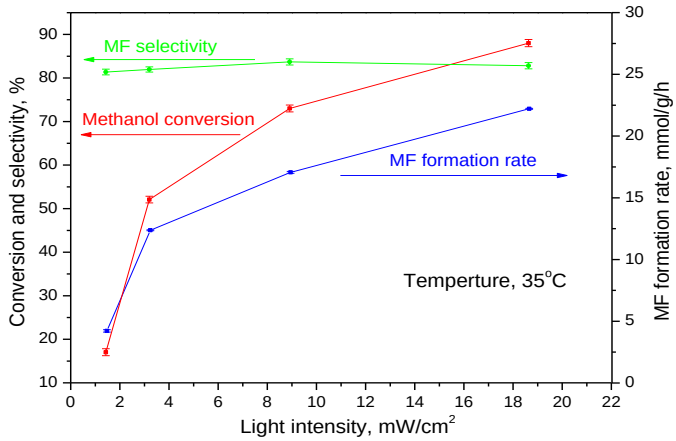

Fig. 7 Influence of light intensity on conversion of methanol, selectivity and formation rate of methyl formate on the catalyst of AuAg(1:1)/TiO_2. The reaction temperature was 35 °C, and the oxygen and methanol volume contents in the feed gas were 0.5 vol.% and 1 vol.%, respectively.

The light intensity had only slight influence on the selectivity of methyl formate but remarkable influence on the methanol conversion, and thus the methyl formate formation rate (Fig. 7). The methanol conversion and the methyl formate formation rate increased nonlinearly with increasing the light intensity, especially in the region of low light intensity. That the light intensity did not influence the selectivity of methyl formate but the methanol conversion indicates that the photo-excited process might not be the rate-determining step.

The high conversion of methanol and the high selectivity to methyl formate of the catalysts are resulted from the special structures of the catalysts. Gold and silver have similar atomic configuration $5d^{10}6s^1$ and $4d^{10}5s^1$. The conduction bands or the highest occupied molecular orbitals (HOMO) and the lowest unoccupied molecular orbitals (LUMO) of gold and silver are formed by the hybridization of *s* and *p* orbitals. However, the formation of the HOMO and LUMO of the Au-Ag alloy is far complicated. The work function of gold (φ_{Au}=5.30 eV) is larger than that of silver (φ_{Ag}=4.26 eV). In the bonding process between gold and silver the electron transfer from silver to gold occurs in order to maintain an equal Femi energy level or chemical potential in the alloy. It has been reported that the flow of *s* electron charge onto the Au sites upon alloying[41, 42] was accompanied by a compensating depletion of 5*d* charge[30]. The DFT study indicates that there exist substantial charge transfer from the 5*s* state of silver to gold, and the charge transfer from the 6*s* and 5*d* states to 6*p* state in Au and that from the 5*s* and 4*d* states to 5*p* state in Ag, resulting in the *spd* hybridization in Au and Ag[32]. As a result, the electronic density in the HOMO of the alloy is higher than that in pure gold or silver. Scheme 1 schematically shows the electronic band structure of gold and silver, as well as the formation process of the band structure of Au-Ag alloy.

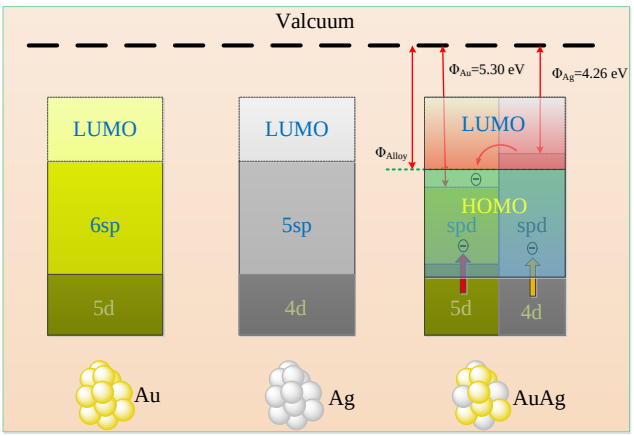

Scheme 1 Schematic profile showing the band structure of gold, silver and the band formation of Au-Ag alloy. The HOMO and LUMO in pure gold and pure silver are formed by the 6*sp* and 5*sp* hybridization, respectively. In Au-Ag alloy, electrons from the 5s orbitals flow onto the Au sites first in order to obtain an equal chemical potential between gold and silver. Partial electron transfer from the 6*s*, 5*d* states to the 6*p* state in Au and from the 5*s*, 4*d* states to 5*p* in silver occurs to form the *spd* hybridization, respectively. The electron density in the HOMO of the Au-Ag alloy is higher than that in pure Au or Ag.

The contact of gold or silver with the surface of titania involves a redistribution of electric charges and the formation of Schottky barriers at the interface between metal and titania[14, 43]. Scheme 2a-c illustrates the formation of Schottky barriers at the interfaces between gold and titania, silver and titania and Au-Ag alloy and titania, as well as the electron transfer mechanisms of the catalysts during the selective oxidation of methanol by oxygen. The noble metal such as gold or silver and titania have different Femi level positions, and the noble metal has a higher work function than titania. When the noble metal and titania are connected electronically, electron migration from titania to the noble metal occurs until the two Femi levels are aligned[14, 43, 44]. As a result, excess negative charges exist at

View Article Online
DOI: 10.1039/C4GC00367E
Journal Name

the metal site of the interface and excess positive charges exist at the titania site of the interface, the Schottky barriers being formed together with the bands of titania bending upward surface. The formation of the Schottky barrier enhances the negative potential of the metal and thus the reducing capacity.

Methanol molecules can be chemisorbed on the surface of titania and partly dissociate to methoxy groups at room temperature [3, 45]. However, no methyl formate or other products could be detected on titania and only trace methyl formate was observed on the catalyst of Au, Ag or Au-Ag alloy nanoparticles supported on titania at the 15 °C to 45 °C temperature range without UV irradiation. The noble metal nanoparticles and/or their perimeters must play a role during the thermal reaction. The reaction mechanism for methanol oxidation on the surface of Au or Ag follows a two-step process involving the initial activation of O-H bonds of methanol followed by the cleavage of the C-H bonds [6, 46]. Each of the two steps involves the dissociative oxygen atoms on the surface of the noble metal. However, studies on the single-crystal Au surface have shown that the dissociation probability for O_2 is less than 10^{-6} [47]. The Schottky barriers (See Scheme 2d) might play an important role for the dissociation of O_2 since the negative charges at the metal site near the perimeter of the interface can attract and dissociatively chemisorb oxygen, while the positive charges at the support site near the perimeter of the interface are favourable to the formation of coordinated methoxy from methanol. The hydrogen from the C-H bonds in the coordinated methoxy reacts with the dissociative oxygen from the surface of the metal by spillover to form coordinated formaldehyde that reacts with excess coordinated methoxy to methyl formate. Like the studies in literature[3], the hydrogen abstraction from methoxy is a rate determining step in the thermal condition, and it is very slow below 45°C so that trace methyl formate was obtained.

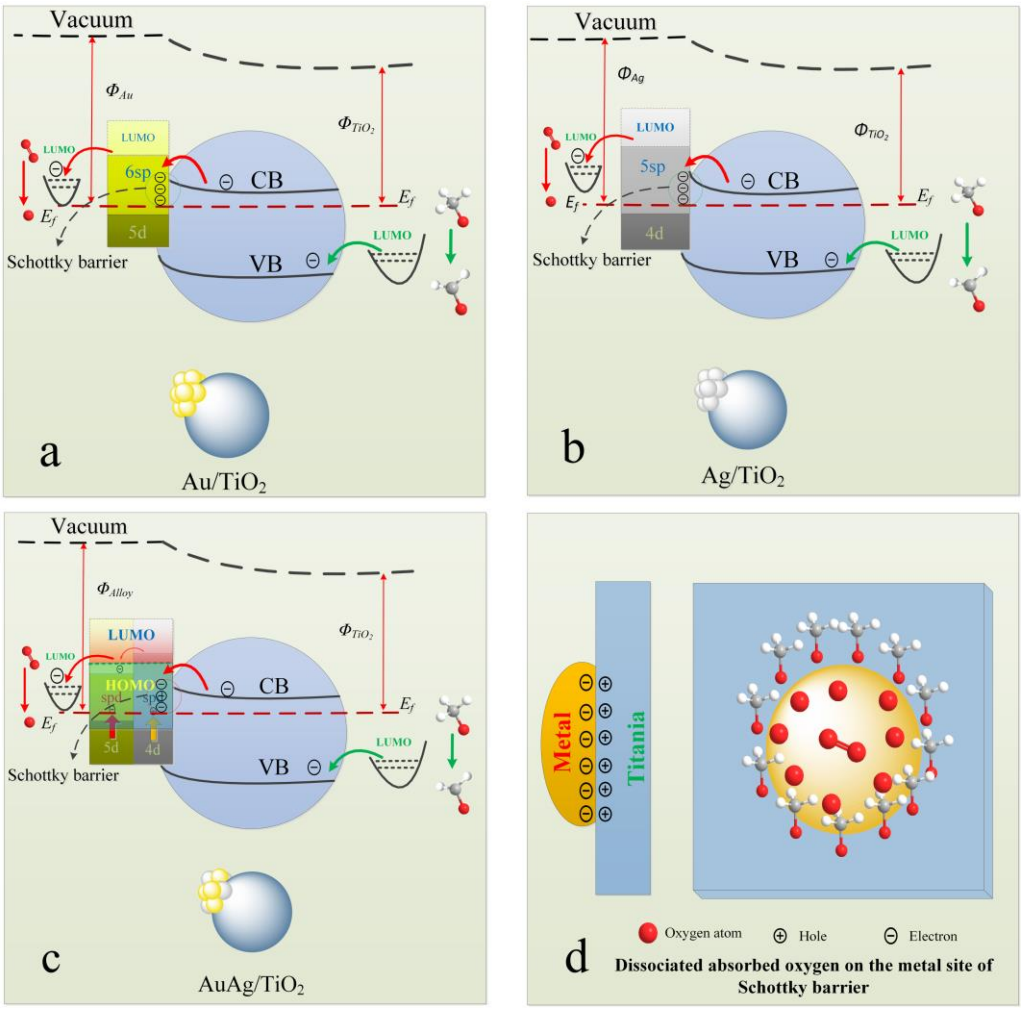

Scheme 2 Schematic profile showing the formation of the Schottky barrier, the band bending, the electron transfer under UV irradiation and the oxygen dissociation on the metal surface near the perimeter. (a-c) Under UV irradiation, the excited electron from the valence band to the conduction band ejects to the metal, together with the exited electrons from intraband and interband transition of the metal, making the metal surface more negative. The negative charge attracts oxygen and induces oxygen dissociation on the surface of metal. The hole on the surface of titania captures electron from the coordinated methoxy to give rise to coordinated formaldehyde due to the higher redox potential of the hole. (d) Oxygen is dissociatively chemisorbed at the perimeter of the metal due to the negative charge in the metal site of the Schottky barrier. Methanol is dissociatively chemisorbed on the positive charged perimeter of the titania sites.

However, the methanol conversion and the selectivity to methyl formate increased sharply on the Au, Ag and Au-Ag alloy supported catalysts and even on the unloaded titania under UV irradiation. As aforementioned above, the formation of

View Article Online
DOI: 10.1039/C4GC00367E

methoxy from methanol can undergo on titania at the room temperature without UV irradiation, water being formed as a by-product[3, 45], which, however, will consume the surface hydroxyls that must be compensated by the oxygen atoms. But the dissociative oxygen is hard to be generated at the reaction temperature without irradiation except the small amount near the perimeters of the Schottky barriers. On the other hand, further reaction from coordinated methoxy to coordinated formaldehyde is hard to undergo as well under the current thermal condition. In the case of UV irradiation, the electrons in the valence band of titania are excited to the conduction band, the electron-hole pairs being created. The coordinated methoxy is then oxidized to the coordinated formaldehyde by the hole since its redox potential is more positive than that of the coordinated methoxy, water or hydroxyl being formed as a by-product. The coordinated formaldehyde reacts with the excess methoxy, giving rise to methyl formate. Oxygen attracted by the excited electrons on the surface of titania (P25) or noble metal nanoparticles gives rise to dissociative oxygen. The dissociative oxygen atom refills the oxygen vacancy resulted from the removal of the surface hydroxyl that reacts with the hydrogen from methanol or methoxy to form water by spillover and diffusion. That there exist only methyl formate and carbon dioxide in the products indicates that once the coordinated formaldehyde is generated it is consumed right away before being released from the surface of titania, and thus the coupling of methoxy and formaldehyde as well as the further oxidation from formaldehyde to carbon dioxide are fast steps under UV irradiation, while the differences of the methanol conversions and the methyl formate selectivities between the catalysts indicate that the dissociation of oxygen is the rate determining step and the spillover and diffusion process is a fast step. The number of the excited electrons on the surface of the alloy nanoparticles is more than that of the Au or Ag nanoparticles under UV irradiation due to the *spd* hybridization of the alloy, the electron transfer from titania to the alloy to form the Schottky barrier, as well as the electron injection from the conduction band of titania to the alloy and the interband and intraband transitions in the alloy by the UV excitation. The electrons in the conduction band of silver are easier to be exited to its surface than that of gold under UV irradiation because the work function of silver is smaller than that of gold. Accordingly, under UV irradiation the oxygen dissociative capability on the alloy nanoparticles is higher than that on Ag or Au nanoparticles, and that on Ag nanoparticles is higher than that on Au nanoparticles. According to the methyl formate formation rate from low to high in Fig. 5a, the catalysts can be categorized into three groups: I unloaded titania, II pure metal supported catalysts, III alloy supported catalysts. The sequence is in line with the oxygen dissociative capacities of the catalysts. In addition, the possibility of methanol chemisorption and dissociation on the noble metal surfaces is very low under UV irradiation because the methanol molecules abhor the negative charged metal surfaces.

In order to verify the roles of the noble metal nanoparticles as well as the surface hydroxyls, we prepared a reference catalyst of AuAg(1:1)/ZnO which was the Au-Ag alloy nanoparticles with an Au/Ag ratio of 1:1 supported on ZnO. The XRD patterns of ZnO and AuAg(1:1)/ZnO are shown in Fig. s4. Zinc oxide is a semiconductor with a band gap of 3.1 eV similar to titania (Fig. s5). And there are also hydroxyls on the surface of ZnO[48]. However, only trace methyl formate was observed during the thermal or photocatalytic reaction in the temperature range from 15 °C to 45 °C on this catalyst (Fig. s6). On the other hand, almost no methyl formate could be observed on the unsupported ZnO. The results, together with those of the catalysts supported on titania, indicate that the noble metal nanoparticles on titania or zinc oxide, unlike the nanoporous gold catalyst[6], play a negligible role in the formation of coordinated methoxy and coordinated formaldehyde during the thermal or photocatalytic reaction, and the chemistry of the hydroxyls existing in several forms[48] on the surface of zinc oxide might be different from those on the surface of titania, which, unlike the latter, plays no role in the reaction.

In addition, the photocatalytic reaction was also performed under visible light irradiation in order to investigate the effect of the LSPR on the reaction. Unfortunately, only trace methyl formate could be observed on the catalysts. This is because that the wavelength of light absorbed by the electrons to induce the LSPR was between 500 nm and 700 nm, and the redox potential of the dipoles resulted from visible light in this band is not high enough to oxidize the methanol molecule and/or methoxy. Accordingly, the LSPR plays no role in the reaction on these catalysts during visible light irradiation.

As aforementioned, the oxygen partial pressure is a sensitive factor during the reaction, which remarkably influences the methanol conversion and the methyl formate selectivity. When oxygen in the feed gas coincides with the stoichiometric ratio, the dissociative oxygen from the surface of noble metal nanoparticles just compensates the oxygen vacancies formed during the reaction, thus further oxidation of the coordinated formaldehyde is hard to occur, resulting in the highest methyl formate selectivity. In the case of lean oxygen, the amount of coordinated formaldehyde resulted from the oxidation of coordinated methoxy decreased, resulting in a sharp decrease of methanol conversion and a slight decrease of the methyl formate selectivity. When oxygen is overdosed, excess dissociative oxygen from the metal surface by spillover deep oxidizes the coordinated methoxy and formaldehyde to carbon dioxide, resulting in high methanol conversion and low methyl formate selectivity. The results further indicate the dissociation of oxygen on the metal surface is the rate-determining step.

Scheme 3 shows the schematic reaction mechanism for the selective oxidation of methanol to methyl formate on the surface of the noble metal supported catalyst. The hydrogen from the O-H bond of the methanol molecule combines with the surface hydroxyl to form water. This process can occur at room temperature in the thermal condition, and be enhanced under UV irradiation. Oxygen is attracted by the negative charge on the surfaces of the metal nanoparticles and dissociatively chemisorbed on them, and then the dissociative oxygen spills over to the oxygen vacancy on the surface of titania, resulted from the removal of the hydroxyl that is consumed to form water. The water formed during the reaction has the negative effect on the methanol conversion in the thermal reaction [2, 3] because it covers the active sites. But such a negative effect was not observed during the photocatalysis because the oxygen vacancy on the surface of titania prefers combining with the dissociative oxygen to the water molecule. The water formed during the reaction is soon carried away by the effluent because of the low partial pressure of water. Once a hole is generated near the methoxy under UV irradiation, an electron in the HOMO of the coordinated methoxy is exited and transferred through its LUMO to the hole, resulting in the breakage of the C-H bond of the coordinated methoxy, and thus the formation of the coordinated formaldehyde. The hydrogen from the C-H bond combines with the bridge-bonding oxygen

View Article Online
DOI: 10.1039/C4GC00367E
Journal Name

on the surface of titania to form the surface hydroxyl. The coordinated formaldehyde rapidly reacts with the excess neighbour methoxy to give rise to methyl formate, or the deep oxidation from formaldehyde through formate to carbon dioxide will undergo. Accordingly, the density of the methoxy on the surface of titania must be high enough in order to achieve a high methyl formate selectivity.

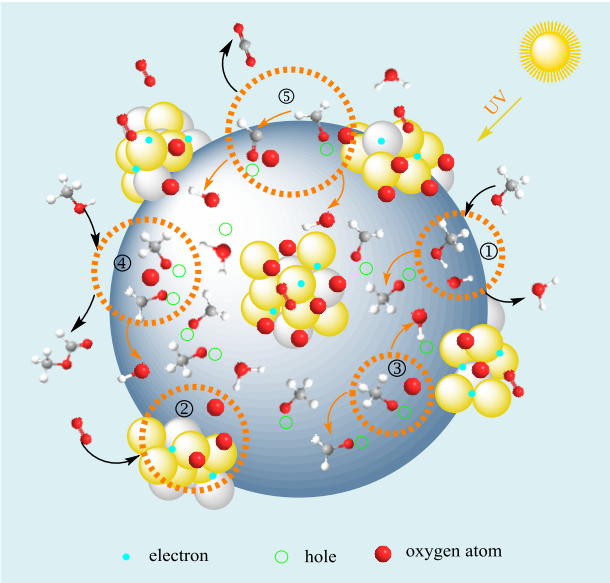

Scheme 3 Schematic reaction mechanism for the selective oxidation of methanol to methyl formate under UV irradiation. (1) The hydrogen from the O-H bond of the methanol molecule combines with the surface hydroxyl to form a water molecule and the chemisorbed methoxy. (2) Oxygen dissociatively chemisorbed on the surface of the metal nanoparticles spillovers to the oxygen vacancy on the surface of titania. (3) The hydrogen from the C-H bond of the chemisorbed methoxy reacts with the bridge bonding oxygen on the surface of titania to form hydroxyl and chemisorbed formaldehyde. (4) The chemisorbed methoxy reacts with the chemisorbed formaldehyde to give rise to methyl formate. (5) The hydrogen atoms from the C-H bonds of the chemisorbed formaldehyde combine with the bridge bonding oxygen to give rise to a carbon dioxide and two hydroxyls.

Conclusions

The catalyst of Au or Ag nanoparticles supported on titania was prepared by the free protecting agent sol immobilization method, and the catalyst of the Au-Ag alloy nanoparticles supported on titania was prepared by the method of partly substitution of silver on titania with gold. The noble metal supported catalyst exhibited the superior methanol conversion and methyl formate selectivity for selective oxidation of methanol by low partial pressure oxygen in air under UV irradiation at the temperature range from 15°C to 45°C, especially for the Au-Ag alloy catalyst of AuAg(1:1)/TiO_2, which was with the highest methanol conversion up to 90% and the selectivity to methyl formate up to 85%. The only by-product was CO_2. The unloaded titania exhibited the lowest methanol conversion of about 20% and methyl formate selectivity of about 50%. The superior photocatalytic performances of the noble metal supported catalysts were closely related to the special structure of the catalyst and the electronic property of the alloy, which enhanced the separation efficiency of the electron-hole pairs by transferring the photo-exited electrons in time from the conduction band of titania to the metal on the one hand, and elevated the negative charge level of the alloy surface by the *spd* hybridization, the formation of Schottky barriers, the electron transfer from the conduction band of titania to metal, and the interband and intraband electron transitions under UV irradiation on the other hand. The photo-generated holes were responsible for the oxidation from methanol to coordinated methoxy, from coordinated methoxy to coordinated formaldehyde and finally to carbon dioxide. The coupling between coordinated methoxy and coordinated formaldehyde to methyl formate was a fast step. The methyl formate selectivity was relevant to the density of the surface methoxy. To enhance the electron-hole separation efficiency was beneficial to the formation of the coordinated methoxy and formaldehyde, and thus enhanced the selectivity to methyl formate. The negative charges on the surface of the metal were responsible for the dissociation of oxygen which was the rate-determining step during the reaction. The dissociative oxygen repelled the water molecules formed from the surface hydroxyls and refilled the oxygen vacancies on the surface of titania. The surface oxygen was responsible for the hydrogen transfer from methanol and methoxy and thus beneficial to the formation of the coordinated methoxy and coordinated formaldehyde. The oxygen partial pressure remarkably influences the methanol conversion and the methyl formate selectivity, while the light intensity has only a significant impact on the methanol conversion but not on the methyl formate selectivity.

Experimental details

P25(Degussa) was purchased from J & K Scientific. $HAuCl_4$, $NaBH_4$ and $AgNO_3$ were purchased from Sinopharm Chemical Reagent Co. Ltd. All chemicals were used as received.

Catalyst Preparation

In a typical procedure, a half gram of the commercial titania P25 (Degussa) was ultrasonically dispersed in deionized ice-water, continuously stirring for 5 min after a suitable amount of solid $NaBH_4$ was added to the suspension in ice bath. Then a suitable amount of the ice-cold $AgNO_3$ ($HAuCl_4$) solution of 5×10^{-3} mol/l was added portionwise to the suspension, continuously stirring for 24 hr. The pure noble metal catalyst of Ag//TiO_2 (Au//TiO_2) was obtained after washing, drying and calcination at 400 °C for 1 h in nitrogen. For Au-Ag alloy, the as-prepared (undried) Ag//TiO_2 was re-dispersed in deionized water and a suitable amount of the $HAuCl_4$ solution of 1×10^{-3} mol/l was added dropwise in the suspension. Then an excess aqueous solution of ammonia was added to the suspension after continuously stirring for 30 min in order to remove AgCl resulted from the gold silver substitution reaction, i.e., equation (1). The solid of Ag@Au core-shell nanoparticles supported on titania was obtained after centrifugation, washing with water and ethanol, and drying. Then the supported Au-Ag alloy catalyst was obtained after the calcination at 400 °C for 1 h in nitrogen. The alloy catalysts calcined at 400 °C at different Au/Ag ratios were labelled as AuAg(1:1)/TiO_2, AuAg(3:1)/TiO_2 and AuAg(1:3)/TiO_2. The catalyst with the Au/Ag ratio 1:1 and calcined at 450 °C for 5 h was labelled as AuAg(1:1)/TiO_2-450C-5. The uncalcined catalyst with the

View Article Online
DOI: 10.1039/C4GC00367E

Au/Ag ratio 1:1 was labelled as AuAg(1:1)/TiO_2-UC. The dealloyed AuAg(1:1)/TiO_2 catalyst was labelled as AuAg(1:1)/TiO_2-A. The schematic preparation procedure of the supported Au-Ag alloy catalysts is shown in Fig. 8.

$$3Ag+HAuCl_4 \rightarrow Au+3AgCl+HCl \quad (1)$$

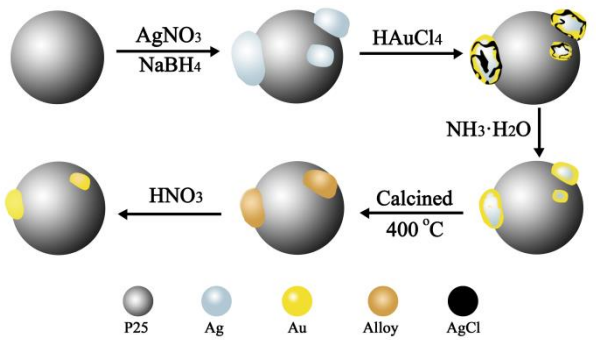

Fig. 8 Schematic preparation procedure of Au-Ag alloy nanoparticles on titania

Catalyst Characterization

X ray diffraction (XRD) measurements were performed using a PANalytical B.V. Empyrean diffractometer with a Cu Kα radiation operated at 40 kV, 40 mA. The scanning range (2θ) of was 5-80 °.The morphology of the samples was investigated by a FEI Tecnai S-Twin transmission electron microscopy (TEM). Light absorbance was measured by a UVIKON/XL UV–vis diffuse reflectance spectrometer (UV-vis) with a scanning range of 200-800 nm. The metal content was measured by the energy-dispersive spectrometry (EDS) using the Brucker-QUANTAX 200 microanalysis system equipped on a Hitachi S-4800 field emission scanning electron microscope (SEM).

Photocatalytic Reaction

The photocatalytic activity of the catalyst was performed in a continuous flow aluminum alloy reactor with a rectangle quartz window on the top and a dividing wall type heat exchanger connected to the back of the bottom of the reactor (Fig. 1s). A piece of rectangle glass which was used as the catalyst holder coating by the catalyst of 0.02 g was installed in the bottom of the reactor, with a thermocouple fixed in touch with the catalyst holder. The cooling water flew through the heat exchanger to maintain a constant temperature. A 500 W high pressure mercury lamp with a cooling jacket, peaking at 365 nm, was positioned 2 cm over the quartz window of the reactor. A gas mixture containing 1 vol.% methanol, 0.5 vol.% O_2, 98.5 vol.% N_2 was supplied at a flow rate of 50 ml/min in the reactor. The reaction temperature was controlled between 15 °C and 45 °C. The products were qualified by a GC-MS in batches and quantified on line by a Shimadzu GC2014C equipped with a FID detector. The formation rate of methyl formate was calculated by the following equation (2).

$$Fr = \frac{\rho V C S}{M \times 2 \times m} \quad (2)$$

where

Fr formation rate, $mmol.g^{-1}.h^{-1}$
ρ concentration of methanol in feed gas, 13 $mg.L^{-1}$
V flow rate of feed gas, 3 $L.h^{-1}$
C conversion of methanol, %
S selectivity of methyl formate, %
M molecular weight of methanol, 32.04 g/mol
m weight of catalyst, 0.02 g

Acknowledgements

The work was financially supported by the key project of Inner Mongolia Education Department (NJZZ13002), the project of Grassland Talent of Inner Mongolia and the project of the western light from the ODPC of Inner Mongolia.

Notes and references

School of Chemistry and Chemical Engineering, Inner Mongolia University, Hohhot, Inner Mongolia, 010021, P. R. China
E-mail: xzyang2007@yahoo.com; Fax: +86 471 6578855; Tel: +86 471 4992982

† Electronic Supplementary Information (ESI) available: Recipe of the catalysts, schematic photocatalytic reactor, TEM images of the AuAg(1:3)/TiO_2, AuAg(3:1)/TiO_2 and the methyl formate formation rate calculated by per unit noble metal, XRD patterns of ZnO and AuAg(1:1)/ZnO, UV-visible spectra of ZnO and AuAg(1:1)/ZnO and GC spectra of AuAg(1:1)/ZnO and AuAg(1:1)/TiO_2. See DOI: 10.1039/b000000x/

1. S. P. Tonner, D. L. Trimm, M. S. Wainwright and N. W. Cant, *Industrial & engineering chemistry product research and development*, 1984, **23**, 384-388.
2. E. Tronconi, A. S. Elmi, N. Ferlazzo, P. Forzatti, G. Busca and P. Tittarelli, *Industrial & engineering chemistry research*, 1987, **26**, 1269-1275.
3. A. S. Elmi, E. Tronconi, C. Cristiani, J. P. Gomez Martin, P. Forzatti and G. Busca, *Industrial & engineering chemistry research*, 1989, **28**, 387-393.
4. M. Ai, *Journal of Catalysis*, 1982, **77**, 279-288.
5. H. Liu and E. Iglesia, *The Journal of Physical Chemistry B*, 2005, **109**, 2155-2163.
6. A. Wittstock, V. Zielasek, J. Biener, C. M. Friend and M. Baumer, *Science*, 2010, **327**, 319-322.
7. J. Liu, E. Zhan, W. Cai, J. Li and W. Shen, *Catalysis Letters*, 2007, **120**, 274-280.
8. Y. Zhao, Z. Qin, G. Wang, M. Dong, L. Huang, Z. Wu, W. Fan and J. Wang, *Fuel*, 2013, **104**, 22-27.
9. H. Kominami, H. Sugahara and K. Hashimoto, *Catalysis Communications*, 2010, **11**, 426-429.
10. X. Yang, A. Zhang, G. Gao, D. Han, C. Han, J. Wang, H. Lu, J. Liu and M. Tong, *Catalysis Communications*, 2014, **43**, 192-196.
11. X. Chen and S. S. Mao, *Chemical reviews*, 2007, **107**, 2891-2959.
12. M. K. Seery, R. George, P. Floris and S. C. Pillai, *Journal of Photochemistry and Photobiology A: Chemistry*, 2007, **189**, 258-263.
13. A. Dawson and P. V. Kamat, *The Journal of Physical Chemistry B*, 2001, **105**, 960-966.
14. M. Jakob, H. Levanon and P. V. Kamat, *Nano Letters*, 2003, **3**, 353-358.

View Article Online
DOI: 10.1039/C4GC00367E
Journal Name

15. I. Paramasivam, J. M. Macak and P. Schmuki, *Electrochemistry Communications*, 2008, **10**, 71-75.
16. E. A. Al-Arfaj, *Superlattices and Microstructures*, 2013, **62**, 285-291.
17. D. Gong, W. C. J. Ho, Y. Tang, Q. Tay, Y. Lai, J. G. Highfield and Z. Chen, *Journal of Solid State Chemistry*, 2012, **189**, 117-122.
18. V. Iliev, D. Tomova, L. Bilyarska, A. Eliyas and L. Petrov, *Applied Catalysis B: Environmental*, 2006, **63**, 266-271.
19. Z. Ji, M. N. Ismail, D. M. Callahan, E. Pandowo, Z. Cai, T. L. Goodrich, K. S. Ziemer, J. Warzywoda and A. Sacco, *Applied Catalysis B: Environmental*, 2011, **102**, 323-333.
20. J. Ménesi, R. Kékesi, A. Oszkó, V. Zöllmer, T. Seemann, A. Richardt and I. Dékány, *Catalysis Today*, 2009, **144**, 160-165.
21. A. Primo, A. Corma and H. Garcia, *Physical chemistry chemical physics : PCCP*, 2011, **13**, 886-910.
22. M. Zhu, G. Qian, G. Ding, Z. Wang and M. Wang, *Materials Chemistry and Physics*, 2006, **96**, 489-493.
23. F. Chen and R. L. Johnston, *Plasmonics*, 2009, **4**, 147-152.
24. T. A. El-Brolossy, T. Abdallah, M. B. Mohamed, S. Abdallah, K. Easawi, S. Negm and H. Talaat, *The European Physical Journal Special Topics*, 2008, **153**, 361-364.
25. S. Link and M. A. El-Sayed, *The Journal of Physical Chemistry B*, 1999, **103**, 8410-8426.
26. S. Sarina, S. Bai, Y. Huang, C. Chen, J. Jia, E. Jaatinen, G. A. Ayoko, Z. Bao and H. Zhu, *Green Chemistry*, 2014, **16**, 331.
27. H. Zhu, X. Chen, Z. Zheng, X. Ke, E. Jaatinen, J. Zhao, C. Guo, T. Xie and D. Wang, *Chemical communications*, 2009, 7524-7526.
28. X. Chen, Z. Zheng, X. Ke, E. Jaatinen, T. Xie, D. Wang, C. Guo, J. Zhao and H. Zhu, *Green Chemistry*, 2010, **12**, 414.
29. H. Zhu, X. Ke, X. Yang, S. Sarina and H. Liu, *Angewandte Chemie*, 2010, **122**, 9851-9855.
30. R. Watson, J. Hudis and M. Perlman, *Physical Review B*, 1971, **4**, 4139-4144.
31. S. Link, Z. L. Wang and M. El-Sayed, *The Journal of Physical Chemistry B*, 1999, **103**, 3529-3533.
32. X.-j. Kuang, X.-q. Wang and G.-b. Liu, *Journal of Alloys and Compounds*, 2013, **570**, 46-56.
33. D. Tsukamoto, A. Shiro, Y. Shiraishi, Y. Sugano, S. Ichikawa, S. Tanaka and T. Hirai, *ACS Catalysis*, 2012, **2**, 599-603.
34. M. J. Chaichi, S. N. Azizi and M. Heidarpour, *Spectrochimica acta. Part A, Molecular and biomolecular spectroscopy*, 2013, **116**, 594-598.
35. P. Geenen, H. J. Boss and G. Pott, *Journal of Catalysis*, 1982, **77**, 499-510.
36. A. Wang, Y. Hsieh, Y. Chen and C. Mou, *Journal of Catalysis*, 2006, **237**, 197-206.
37. A. Zielińska-Jurek, E. Kowalska, J. W. Sobczak, W. Lisowski, B. Ohtani and A. Zaleska, *Applied Catalysis B: Environmental*, 2011, **101**, 504-514.
38. K. Ueno and H. Misawa, *Journal of Photochemistry and Photobiology C: Photochemistry Reviews*, 2013, **15**, 31-52.
39. E. Kowalska, O. O. Mahaney, R. Abe and B. Ohtani, *Physical chemistry chemical physics : PCCP*, 2010, **12**, 2344-2355.
40. S. Qin, F. Xin, Y. Liu, X. Yin and W. Ma, *Journal of colloid and interface science*, 2011, **356**, 257-261.
41. P. H. Barrett, R. W. Grant, M. Kaplan, D. A. Keller and D. A. Shirley, *The Journal of Chemical Physics*, 1963, **39**, 1035-1040.
42. L. D. Roberts, R. L. Becker and F. Obenshain, *Phys. Rev. A*, 1965, **137**, 895.
43. A. L. Linsebigler, G. Lu and J. T. Yates Jr, *Chemical reviews*, 1995, **95**, 735-758.
44. E. H. Rhoderick and R. Williams, *Metal-semiconductor contacts*, Clarendon Press Oxford, 1988.
45. G. Ramis, G. Busca and V. Lorenzelli, *Journal of the Chemical Society, Faraday Transactions 1: Physical Chemistry in Condensed Phases*, 1987, **83**, 1591-1599.
46. X. Liu, R. J. Madix and C. M. Friend, *Chemical Society Reviews*, 2008, **37**, 2243.
47. X. Deng, B. K. Min, A. Guloy and C. M. Friend, *Journal of the American Chemical Society*, 2005, **127**, 9267-9270.
48. H. Noei, H. Qiu, Y. Wang, E. Loffler, C. Woll and M. Muhler, *Physical chemistry chemical physics : PCCP*, 2008, **10**, 7092-7097.